Journal of Integrative Agriculture 2026, 25(9): 3786–3799

Available online at ScienceDirect

Journal of Integrative Agriculture

RESEARCH ARTICLE

MFAP5 enhances the cold resistance of piglets by promoting the transition of adipocyte progenitor cells to fibroblast lineage

Xiangfei Ma[1], Mengting Li[1], Shengda Qiu[1], Di Liu[2], Hong Ma[2], Wei Wei[1], Lifan Zhang[1], Zan Huang[1#], Jie Chen[1#]

[1] *College of Animal Science and Technology, Nanjing Agricultural University, Nanjing 210095, China*
[2] *Institute of Animal Husbandry, Heilongjiang Academy of Agricultural Sciences, Harbin 150086, China*

Highlights

- Dorsal subcutaneous adipose tissues (subWATs) in piglets exhibited thermogenic potential and fibrotic remodeling under cold stress.
- Single-nucleus RNA-seq (snRNA-seq) and RNA-seq identified *MFAP5* as a critical mediator of cold-induced adipose plasticity, which promoted fibrogenic lineage commitment in fibro/adipogenic progenitors (FAPs).
- *MFAP5* overexpression or conditioned medium inhibited adipocyte differentiation and induced fibroblast-like phenotypes in C3H10T1/2 and porcine stromal vascular fraction (SVF) cells, accompanied by elevated mitochondrial activity.
- *MFAP5* activates the Hippo signaling pathway, thereby increasing the nuclear translocation of YAP1 and upregulating fibrogenic markers such as *ACTA2* and *CTGF*.

Graphical abstract

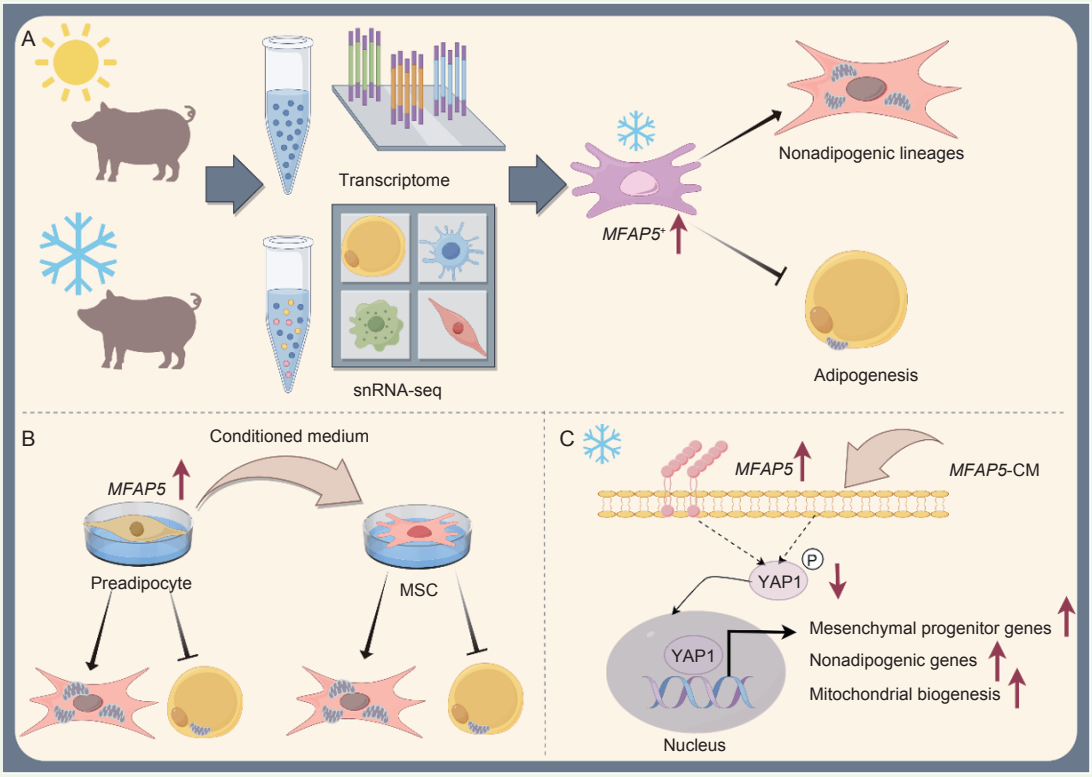

Received 17 February 2025; Received in revised form 27 April 2025; Accepted 1 August 2025; Available online 4 September 2025
Xiangfei Ma, E-mail: 2021205002@stu.njau.edu.cn; #Correspondence Jie Chen, E-mail: jiechen@njau.edu.cn; Zan Huang, E-mail: huangzan@njau.edu.cn

doi: 10.1016/j.jia.2025.09.006

Abstract

Although pigs lack classical brown adipose tissue, several studies have demonstrated that porcine adipocytes possess the capacity to undergo thermogenesis through UCP1-independent mechanisms. However, the developmental processes and regulatory mechanisms underlying these thermogenic adipocytes remain poorly characterized. Here, we found that dorsal subcutaneous adipose tissues (subWATs) in pigs exhibits significant thermogenic potential under cold stress. Notably, we observed substantial cold-induced structural remodeling in dorsal subWATs, characterized by increased fibrotic deposition. An integrated analysis of snRNA-seq and RNA-seq data on dorsal subWATs identified MFAP5, which encodes a microfibril-associated glycoprotein in the extracellular matrix, as a potential regulator of the cold-induced plasticity of dorsal subWATs. Both *MFAP5* overexpression and *MFAP5*-conditioned medium (*MFAP5*-CM) not only inhibited preadipocyte differentiation into adipocytes but also promoted their commitment to non-adipogenic fibrogenic lineages. Furthermore, *MFAP5* treatments significantly enhanced the mitochondrial biogenesis of these fibrogenic cells. Mechanistic investigations showed that these phenotypic alterations are predominantly mediated through the Hippo signaling pathway. In summary, our findings elucidate the pivotal role of *MFAP5* in regulating adipocyte development following cold exposure, thus providing crucial insights into the molecular mechanisms underlying porcine adaptation to cold stress.

Keywords: piglets, cold adaptation, cell fate, microfibril associated protein 5

1. Introduction

Adipose tissue is primarily composed of fibroblasts, endothelial cells, fibro/adipogenic progenitors (FAPs), and mature adipocytes (Norreen-Thorsen *et al.* 2022). Mammalian adipose tissue is an extraordinarily flexible and heterogeneous organ that regulates energy balance. With significant changes in energy requirements, including fasting, feeding, cold, and exercise, adipose tissue exhibits remarkable plasticity, with its metabolism rapidly shifting to meet the energetic needs of the organism (Krois *et al.* 2019; Kotarsky *et al.* 2021; Bornstein *et al*. 2023).

Recent studies have demonstrated the plasticity between adipocyte and fibroblast lineages. The conversion of adipocytes and nonadipogenic fibroblasts due to external stimuli or genetic changes affects the remodeling of adipose tissues. In the ceiling culture method, mature adipocytes are cultured at the top of a culture bottle, where they de-differentiate into preadipocytes (Côté *et al.* 2019). In the dermis, mature adipocytes undergo de-differentiation to produce contractile myofibroblasts (Shook *et al.* 2020). The activation of β-catenin and SOX4 in mesenchymal progenitors impairs the adipogenic capacity of adipose tissue and induces a fate shift toward nonadipogenic lineages (Zeve *et al.* 2012; He *et al.* 2023). However, the mechanisms underlying the conversion between adipocytes and nonadipogenic fibroblast lineages remain poorly understood.

Cold stress in piglets represents a critical challenge in the pig farming industry, and cold stress-induced mortality in piglets can result in significant economic losses in production (Le Dividich *et al.* 1981; Kelley *et al.* 1982). Although brown adipose tissue (BAT) plays a crucial role in thermoregulation and body temperature maintenance (Xiao *et al.* 2023), current evidence indicates that pigs lack functional BAT (Trayhurn *et al.* 1989; Berg *et al*. 2006; Hou *et al.* 2017). However, studies have shown that while pigs generally lack typical BAT, beige adipose tissue has been identified as contributing to thermogenesis in Tibetan and Min pigs. Nevertheless, the mechanisms underlying the cold response in adipose tissue of other pig breeds remain poorly understood (Lin *et al.* 2017; Zheng *et al.* 2017; Hou *et al.* 2018). Collectively, our current understanding of thermogenic mechanisms in pigs under cold exposure remains limited. Therefore, further research is required to elucidate the potential alternative thermogenic mechanisms in pig adipose tissue.

In this study, a cold exposure experiment using Erhualian piglets revealed that the subcutaneous adipose tissues (subWATs) in the dorsal region exhibits thermogenic potential and fibrotic characteristics. Single nucleus RNA sequencing (snRNA-seq) and RNA-seq of the dorsal subWATs were used to investigate the relationship between thermogenesis and fibrosis in piglets. This research provides novel insights into the cold adaptation mechanisms of piglets.

2. Materials and methods

2.1. Animals

The pigs used in this study had *ad libitum* access to a commercial pig diet (with nutrient levels according to the Nutrient Requirements of Swinee (NRS)) and water throughout the experimental period. Erhualian piglets were purchased from Changzhou Erhualian Cooperative, China.

2.2. Cold exposure experiment

A 1-mon cold exposure experiment test was conducted on male piglets aged 6–8 wk with similar body weight. A total of 4 pairs of littermate piglets were divided into the room temperature (RT) group and the cold exposure group, with 4 piglets in each group. The temperature of the room temperature group was (28±0.5)°C, and that of the cold exposure group was (11±0.5)°C (Appendix A). They were feed quantitatively in separate cages. Specifically, the daily feed allowance was calculated based on each piglet's initial body weight (at the start of the experiment) at a standard rate of 1.5 kg d^{-1}, with proportional adjustments made according to weight gain to ensure that both groups received exactly the same total amount of feed daily. All the feed provided feed was completely consumed by the piglets after each feeding.

2.3. Library construction and analysis of RNA-seq and snRNA-seq data

Total RNA was isolated from the subWATs of male piglets in both the RT group and the cold exposure group (n=4 biologically independent samples). RNA libraries were constructed and sequenced on the Illumina Sequencing Platform by BGI Genomics Co., Ltd. (Shenzhen, China). Throughout this study, consistent screening criteria were applied for identifying differentially expressed genes (DEGs) in all bioinformatics analyses. Significantly DEGs were screened under the following conditions: false discovery rate (FDR)<0.05, $|\log_2 FC|>1$, and $P<0.05$. Differential gene expression analysis was performed using the BGI platform (https://biosys.bgi.com/).

Three piglets in the RT group and cold exposure group were mixed with subWATs taken from the dorsal region for snRNA-seq assay (Genedenovo Biotechnology Co., Ltd. (Guangzhou, China, Illumina PE150). The Cell Ranger Single Cell Software Suite was applied for quality control, and snRNA-seq data were aligned to *Sus scrofa* 11.1 as the reference genome. After the initial quality control, low-quality sequences with barcodes and unique molecular identifiers (UMIs) were removed. CellRanger and Seurat R package were used to filter out the low-quality cells: (1) The number of genes identified in a single cell (500–4,000); (2) UMI counts>10,000 per cell; and (3) the percentage of mitochondrial genes in individual cells (less than 5%). The cell numbers obtained for each sample, quality control results, and alignment statistics are provided in Appendices B and C. Data were visualized using Uniform Manifold Approximation and Projection (UMAP) to project the cells into 2D space. Distances between the cells were calculated based on previously identified principal components (PCs). Briefly, Seurat was used to embed cells in a shared-nearest neighbor (SNN) graph, with edges drawn between cells *via* similar gene expression patterns. To partition this graph into highly interconnected quasi-cliques or communities, the SNN graph was first constructed based on the Euclidean distance in principal component analysis (PCA) space and the edge weights between any two cells were refined based on the shared overlap in their local neighborhoods (Jaccard distance). Cells were then clustered using the Louvain method to maximize modularity (default resolution=0.5). The RNA libraries were sequenced on the Illumina sequencing platform by Genedenovo. Bioinformatic analysis was performed using Omicsmart, a dynamic real-time interactive online platform for data analysis (http://www.omicsmart.com). The gene expression matrix was input into Monocle2, and dimension reduction was performed. Cells were organized into a tree-like trajectory that included branches and nodes. Subsequently, the most primitive cell clusters by differentiation state along the trajectory were defined as the cell clusters with the smallest pseudo-time value, then the pseudo-time values for all cells were calculated. Based on the pseudo-time values, Monocle2 was used to construct gene expression patterns as a smooth, nonlinear function of pseudo-time to examine how gene expression changes with pseudo-time. Genes with FDR<1e-5 were selected as the differentially expressed genes (DEGs). Porcine stroma-vascular fraction (SVF) cells were treated with either *MFAP5*-conditioned medium (MFAP5-CM) or control medium (NC-CM) and induced to differentiate for 8 d. The extracted RNA and the RNA libraries were sequenced on the Illumina sequencing platform by Genedenovo. Bioinformatic analysis was performed using Omicsmart.

2.4. Isolation of SVF and differentiation of preadipocytes

SVF cells were collected from the subWATs isolated from freshly slaughtered piglets, following the procedures in our previous report (Lin *et al.* 2020). The differentiation of SVF and immortalized porcine preadipocytes (ISP4#) was performed according to the previously described 4×4 protocol (Cheng *et al.* 2023), as shown in the Appendix D-b.

2.5. Cell lines and culture

C3H10T1/2 differentiation was induced by treating confluent cells for 48 h in a medium containing 0.5 mmol L^{-1} 3-isobutyl-1-methylxanthine (Sangon, China, A606630), 5 μmol L^{-1} dexamethasone (Sangon, A601187), 0.12 μg mL^{-1} insulin (Novolin R), 5 n mol L^{-1} T3 (Makclin, China, T819947) and 1 μmol L^{-1} rosiglitazone (Makclin, China, R832516). Two days after induction, cells were switched to maintenance medium containing 0.12 μg mL^{-1} insulin, 5 nmol L^{-1} T3 and 1 μmol L^{-1} rosiglitazone. The schematic diagram of C3H10T1/2 added with *MFAP5*-CM is shown in Appendix E.

2.6. RNA isolation and RT-qPCR

Total RNA was isolated from cells or tissues using TRIzol (Accurate Biology, China, AG21101) according to the manufacturer's instruction. For reverse transcription, 1 μg RNA was used to generate cDNA using the 5×Evo M-MLV RT Master Mix (Accurate Biology, AG11706) and RT-qPCR was carried out with SYBR qPCR Master Mix on ABI (Applied Biosystems, USA). The relative mRNA levels were calculated with the $2^{-\Delta\Delta CT}$ method and normalized to *RPLP0* mRNA. The primer sequences are listed in Appendix F.

2.7. Oil Red O staining

Cells at the specified stage of differentiation were rinsed with PBS and fixed with 4% formaldehyde in PBS for 20 min. After washing twice in PBS, cells were stained with Oil Red O at RT for 20 min. The cells were washed twice with PBS and photographed. For quantification, the stained adipocytes were incubated with isopropanol for 10 min, and the absorption value of the solution at 510 nm was measured with a spectrophotometer.

2.8. Immunofluorescence

Differentiated ISP4# were fixed with 4% PFA for 15 min, washed with PBS, and blocked with PBS containing 5% BSA and 0.3% Triton X-100 for 1 h at room temperature. They were then incubated with primary antibody YAP1 overnight at 4°C (Proteintech, China, 13584-1-AP), and subsequently with the secondary fluorescent-conjugated antibody (Beyotime, China, A0516) at RT in the dark for 1 h. DAPI was used to visualize the nuclei. Image acquisition was performed with an LSM 900 microscope (Zeiss, Germany).

2.9. Lentiviral production and infection

For constructing the overexpression lentiviral plasmids, the *MFAP5* CDS sequences were cloned into the SmaI sites of the pLVX-V5-IRES-neo vector (the primers for cloning *MFAP5* are shown in Appendix F). To generate lentivirus particles, lentiviral constructs were co-transfected with pM2D. G and psPAX2 into HEK293T cells. Media containing lentivirus was harvested, filtered, and concentrated at 48 h and 72 h post-transfection. Then 60% of confluent ISP4# were incubated with lentivirus premixed with polybrene (10 μg mL^{-1}) (Servicebio, China, G1803) for 72 h. Finally, 800 μg mL^{-1} G418 antibiotic (Beyotime, ST081) was added to screen positive cells, and growth was maintained at 100 μg mL^{-1}.

2.10. Western blotting

Protein was extracted from tissues and cells with RIPA reagent (NCM Biotech, China, WB3100) according to the manufacturer's instructions, and it was supplemented with a phosphatase and protease inhibitors (Beyotime, P1050). Samples were denatured using sodium dodecyl sulfate (SDS) loading buffer (Yeasen Biotech, China, 20315ES20). Total protein was separated by SDS-PAGE and transferred to polyvinylidene fluoride (PVDF) membrane (Millipore, USA, Merck-ISEQ00010). All membranes were then blocked by incubation with 5% BSA in Tris-buffered saline containing Tween-20 (TBST, TBS with 0.1% Tween 20) for 1 h at RT. Membranes were incubated with primary antibodies overnight at 4 °C and then with HRP-conjugated anti-rabbit IgG (Beyotime, A0208), anti-mouse IgG (Beyotime, A0216) secondary antibody for 1 h at room temperature. Enhanced chemiluminescence (ECL) Western blotting substrates (Biosharp, China, BL520B) were used to visualize the results. Images were acquired using the Amersham ImageQuant 800 (Cytiva). The following antibodies were used: Anti-Tubulin (Proteintech, 11224-1-AP), anti-MFAP5 (Affinity, China, DF13146), anti-UCP3 (ABclonal, China, A23285), anti-PPARG (Proteintech, 16643-1-AP), anti-ACTA2 (Proteintech, 67735-1-Ig), anti-HSL, (Proteintech, 17333-1-AP), anti-CPT1A (Proteintech, 15184-1-AP), anti-PRDM16 (Affinity, DF13303), anti-PGC1A (Proteintech, 66369-1-Ig), anti-COX4 (Proteintech, 11242-1-AP), anti-TOM20 (ABclonal, A19403), anti-p44/42 MAPK (ERK1/2) (CST, 4695), anti-phospho-p44/42 MAPK (ERK1/2) (Thr202/Tyr204) (CST, USA, 4370), anti-p38 MAPK (Proteintech, 80821-2-RR), anti-phospho-p38 MAPK (Thr180/Tyr182) (Proteintech, 28796-1-AP), anti-YAP1 (Proteintech, 13584-1-AP), and anti-Phospho-YAP1 (S127) (HuaBio, China, ET1611-69).

2.11. Statistical analysis

All values are expressed as mean±SEM. The error bars (SEM) shown for all results were derived from biological replicates. Results were analyzed by Student's *t*-tests using GraphPad Prism 8.0 software, and *P*-value <0.05 was considered statistically significant.

3. Results

3.1. subWATs on the dorsal side of Erhualian piglets have the potential to resist cold

To investigate the characteristics of porcine adipose tissue in response to cold stimuli, adipose tissue samples were collected from the 2 groups at various anatomical locations, including subWATs in the dorsal region, deep neck, scapula, deep scapula, inguinal fat, deep inguinal fat, perirenal, axillary, frontal neck, and heart fat. In the RT group, all adipose tissue depots exhibited typical white adipose tissue morphology. However, in the cold exposure group, sizes of adipocytes at different anatomical locations showed varying degrees of reduction (Fig. 1-A). Notably, subWATs from the dorsal, inguinal, and deep cervical regions demonstrated significant upregulation of genes associated with lipolysis (*ATGL*, *HSL*) and thermogenesis (*UCP3*, *PGC1A*, *PRDM16*, *TFAM*) (Fig. 1-B), suggesting these adipose depots are particularly responsive to cold-induced thermogenesis. In contrast, subWATs from the remaining 7 adipose depots showed no significant alterations in the expression of lipolysis- and thermogenesis-related genes (Appendix A-e).

Furthermore, histological analysis revealed that dorsal subWATs exhibited distinct morphological alterations compared to the other depots, displaying characteristics resembling murine brown adipose tissue and showing evidence of fibrotic remodeling (Fig. 1-C). Bodipy staining confirmed the adipose nature of these transformed tissues, revealing a significant reduction in lipid droplet content in cold-exposed specimens (Fig. 1-D). Masson staining demonstrated extensive fibrotic remodeling within the adipose tissue (Fig. 1-E). Western blot analysis revealed significant upregulation of thermogenic markers (PRDM16, UCP3, TOM20) and the lipolytic enzyme HSL in dorsal subWATs following cold exposure (Fig. 1-F). *ACTA2*, encoding α-smooth muscle actin, serves as a specific marker for myofibroblasts and plays crucial roles in smooth muscle contraction (Rockey *et al*. 2013; Newman *et al*. 2021). qPCR and Western blot analyses confirmed the significant upregulation of ACTA2 expression in the dorsal subWATs following cold exposure (Fig. 1-F and G).

In vitro, isoproterenol (ISO) and Mirabegron were used to simulate the cold stimulation of SVF cells (Miller *et al.* 2015; Winther *et al.* 2018; O'Mara *et al.* 2020). *PGC1A*, *DIO2*, *PRDM16*, *CD137*, and *UCP3* were significantly upregulated in SVF, and the expression level of the *ACTA2* gene was also significantly upregulated (Fig. 1-H). These results indicate that subWATs on the dorsal side of Erhualian piglets are thermogenic-related fat, and the adipose tissue undergoes fibrosis.

3.2. RNA-seq identified thermogenesis- and fibrosis-related gene signatures in dorsal subWATs

To verify the morphological observations, RNA-seq of subWATs in the dorsal region was performed. A total of 207 DEGs were found in dorsal subWATs after cold exposure, with 166 genes upregulated and 41 genes downregulated (Fig. 2-A). qPCR verification of DEGs were consistent with the sequencing results (Appendix A-f). The results of gene set enrichment analysis (GSEA) showed that the oxidative phosphorylation, thermogenesis, and cardiac muscle contraction pathways were significantly upregulated in the subWATs of the dorsal region under cold stimulation (Fig. 2-B).

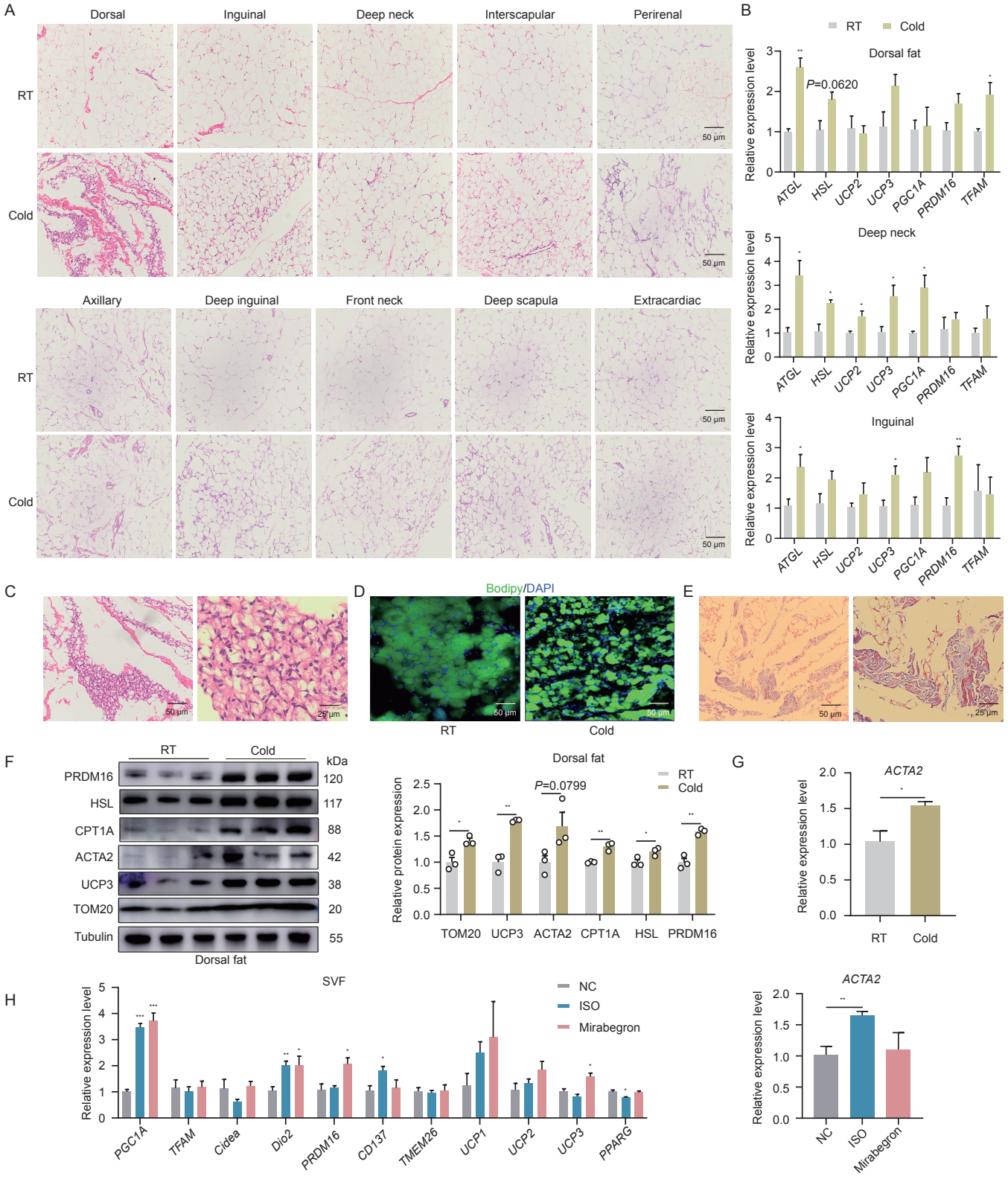

Fig. 1 Responses of adipose tissues from different parts of Erhualian piglets to cold stimulation. A, representative images of H&E-stained adipose tissue sections from Erhualian piglets housed for 1 mon at room temperature (RT) or under cold exposure. Scale bar=50 μm. B, qRT-PCR analysis of thermogenesis-related gene expression in adipose tissue samples (n=3–4 biologically independent samples). C, representative images of H&E-stained subcutaneous adipose tissue (subWAT) slices from the dorsal region of Erhualian piglets under cold exposure. D, representative images of Bodipy-stained subWAT slices from the dorsal region of Erhualian piglets under room temperature or cold exposure conditions. E, representative images of Masson-stained subWAT slices from the dorsal region of Erhualian piglets under cold exposure. F, Western blot analysis of thermogenesis-related gene expression in subWAT samples of the dorsal region (n=3 biologically independent samples). G, qRT-PCR analysis of *ACTA2* gene expression in subWAT samples from the dorsal region of Erhualian piglets at room temperature or under cold exposure (n=4 biologically independent samples). H, qRT-PCR analysis of thermogenesis-related gene and *ACTA2* gene expression in SVF adipocytes treated with isoproterenol (ISO) or Mirabegron (n=4 biologically independent samples). NC, normal control. All numerical values are presented as mean±SEM; two-tailed unpaired Student's t-test P-values are indicated as: *, P≤0.05; **, P≤0.01; ***, P≤0.001.

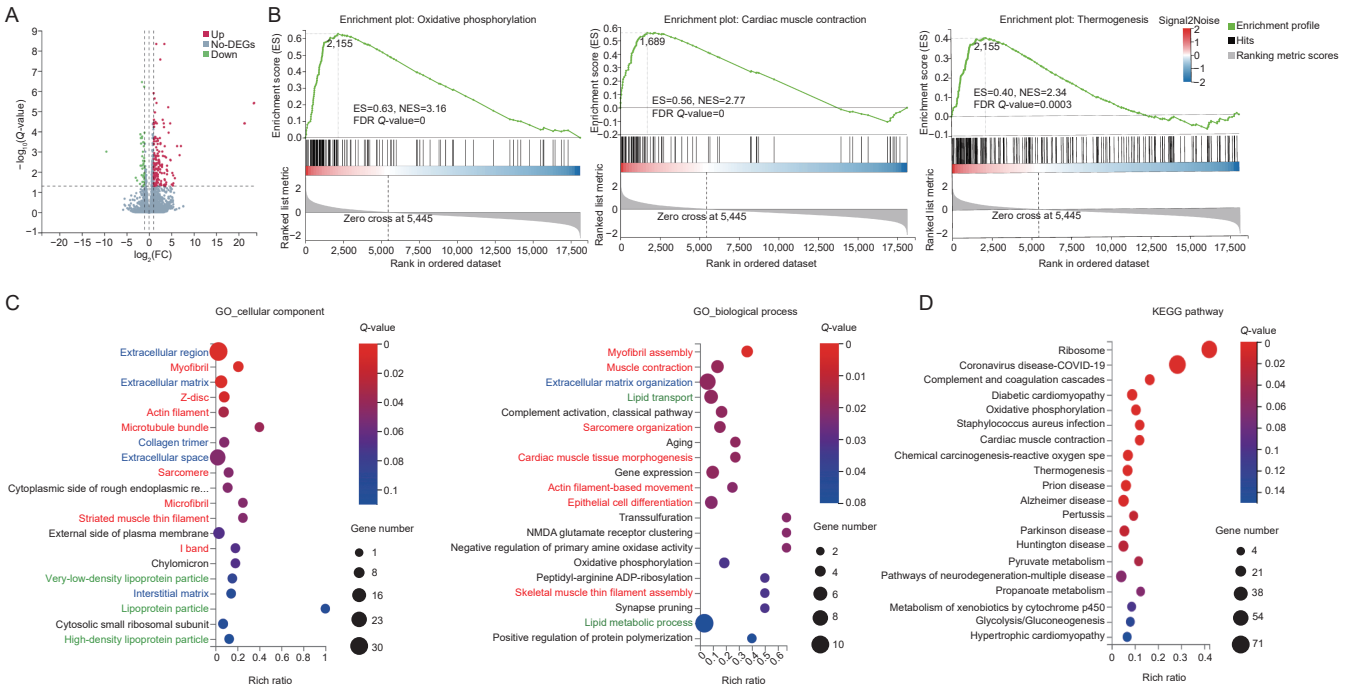

Fig. 2 Gene expression alterations in dorsal subcutaneous adipose tissues (subWATs) are revealed by cold exposure *via* RNA-seq. A, volcano plots showing a global overview of the gene expression profiles of subWATs on the dorsal region of Erhualian piglets. B, gene set enrichment analysis (GSEA) of the enriched pathyways in cold exposure group compared with RT group. C, the top 20 GO terms revealed by GO (cellular composition and biology) enrichment analysis of differentially expressed genes (DEGs). D, the top 20 enrichment pathways revealed by KEGG enrichment analysis of DEGs.

GO enrichment analysis revealed that DEGs are mainly related to myofibril assembly, muscle contraction, extracellular matrix organization, oxidative phosphorylation, and other biological processes. At the cellular component level, differential genes are mainly related to myofibril, extracellular matrix, Z-disc, actin filaments, and others (Fig. 2-C). KEGG enrichment analysis showed that genes related to oxidative phosphorylation, myocardial contraction, and thermogenesis were differentially expressed in the subWATs of the dorsal region after cold stimulation (Fig. 2-D).

3.3. FAPs in subWATs of the dorsal region develop into a nonadipogenic fibroblasts lineage

To establish a comprehensive cellular atlas of dorsal subWATs and characterize their adaptive response to cold stimulation at single-cell resolution, we performed snRNA-seq on dorsal subWAT samples from both the RT and cold exposure groups. Using unsupervised graph-based clustering analysis, we identified 9 distinct cell clusters within the integrated cellular atlas (Fig. 3-A). Based on the highly expressed genes within each cluster and established marker genes (Burl *et al.* 2018; Vijay *et al.* 2020; Norreen-Thorsen *et al.* 2022; Maniyadath *et al.* 2023), these populations were classified as FAPs, adipocytes, endotheliocyte, smooth muscle cells (SMC), Schwann, T cells, macrophages, B cells, and monocytes (Fig. 3-B). The adipocytes (28.36%), FAPs (20.35%), and endotheliocytes (27.89%) constituted the predominant cell populations (Appendix G-a). Comparative analysis demonstrated that cold stimulation induced cellular remodeling in the dorsal subWATs, characterized by a 5.68% reduction in the adipocyte proportion, accompanied by 3.51% and 3.2% increases in the FAPs and endothelial cell populations, respectively (Fig. 3-C).

After the observed FAPs proportional increase, subclustering analysis was further performed to characterize the heterogeneity of FAPs, which identified 8 distinct subpopulations (Fig. 3-D). Gene expression profiling identified FAP0, FAP2, FAP3, FAP4, and FAP6 as adipogenic subpopulations, based on their expression of established adipogenic markers including *LPL*, *PPARG*, *LIPE*, and *ADIPOQ* (Fig. 3-E). In contrast, FAP1, FAP5, and FAP7 were classified as nonadipogenic fibroblast populations, characterized by their expression of adipogenesis-inhibiting factors including *POSTN*, *COL1A1*, *FN1*, and *ZNF521* (Fig. 3-E). FAPs represent mesenchymal-derived interstitial progenitors capable of bidirectional differentiation into both adipogenic and nonadipogenic fibroblast lineages (Cristancho and Lazar 2011). A pseudotemporal trajectory analysis using Monocle2 revealed 2 primary differentiation pathways for porcine FAPs: adipocyte lineage and nonadipogenic fibroblast lineage (Fig. 3-F). Cold exposure significantly altered the composition of FAPs by reducing the adipogenic potential population while enhancing commitment to nonadipogenic fibroblast lineages (Fig. 3-G). Collectively, these findings demonstrate that cold exposure promotes FAP differentiation toward nonadipogenic fibroblast lineages.

Compared to the RT group, the nonadipocyte fibroblast populations (FAP1, FAP5 and FAP7) in the cold exposure

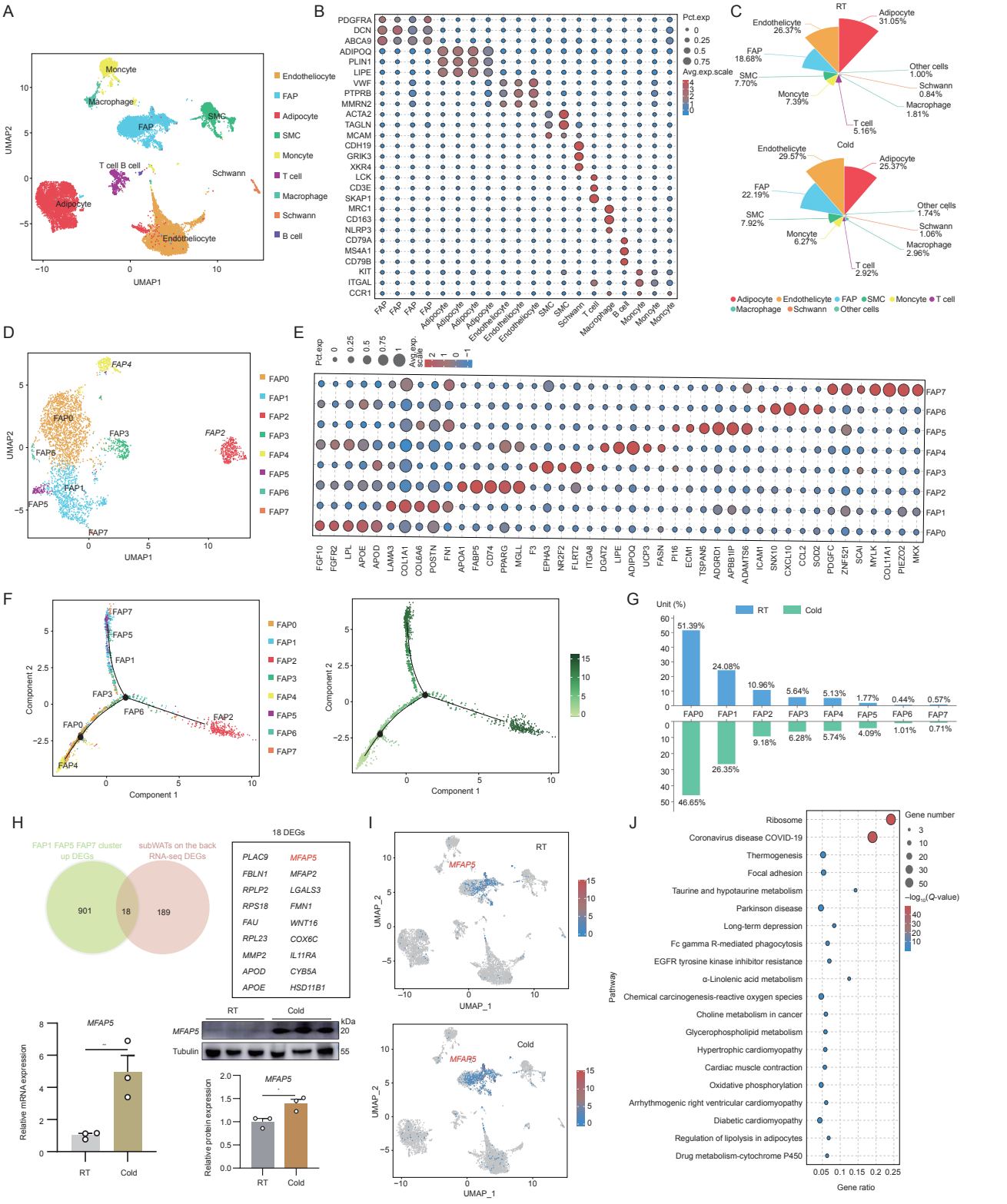

Fig. 3 Cellular compositions in subcutaneous adipose tissues (subWATs) of the dorsal region are altered by cold exposure. A, Uniform Manifold Approximation and Projection (UMAP) of subWAT cell types. B, bubble chart showing scaled average expression levels of selected cell-type-enriched marker genes. C, the fraction of each cell type in subWATs of the dorsal region from the room temperature (RT) group or the cold exposure group. SMC, smooth muscle cell. D, UMAP of fibro/adipogenic progenitor (FAP) subpopulations. E, bubble chart showing scaled average expression of FAP subpopulation-enriched marker genes. F, trajectory inference and state information of FAP subpopulations. G, the fraction of each FAP subpopulation in subWATs of the dorsal region from the RT group or the cold exposure group. H, Venn diagram showing the significantly upregulated overlapping genes for DEGs of the *FAP1, FAP5, and FAP7* cluster and RNA-seq of subWATs in the dorsal region, qRT-PCR and Western blotting analysis of *MFAP5* gene expression in subWAT samples from the dorsal region of Erhualian piglets housed for 1 mon at RT or under cold exposure (n=3 biologically independent samples). I, UMAP of *MFAP5* positive cells. J, the top 20 enrichment pathways revealed by KEGG enrichment analysis of upregulated DEGs in *MFAP5* positive cells. All numerical values are presented as mean±SEM; two-tailed unpaired Student's t-test P-values are indicated as: **, $P \leq 0.01$.

group exhibited a total of 919 upregulated DEGs. Comparative analysis revealed that the nonadipocyte fibroblast lineage exhibited 18 differentially upregulated genes that overlapped with the DEGs identified in the subWATs RNA-seq analysis. Among these overlapping genes, *MFAP5* was identified as a significantly DEG (Fig. 3-H). qPCR and Western blot analyses confirmed the significant upregulation of *MFAP5* expression in dorsal subWATs following cold exposure (Fig. 3-H). *MFAP5* is mainly expressed in the FAPs, with a significant increase in the *MFAP5*-positive cell population observed in the cold exposure group (Fig. 3-I). Furthermore, pathway enrichment analysis of differentially upregulated genes in *MFAP5*-positive cells following cold exposure revealed significant involvement in the thermogenesis, myocardial contraction, and oxidative phosphorylation pathways (Fig. 3-J). These findings suggest that *MFAP5*-positive cell populations in dorsal subWATs may play a crucial role in adaptive responses to cold exposure.

3.4. *MFAP5* promotes FAPs development towards the nonadipogenic lineage

Previous studies have demonstrated that *MFAP5* functions as a secreted protein, with detectable levels in the culture medium of human adipose-derived stem cells (ASCs) (Hoerst *et al.* 2019). To investigate the potential of *MFAP5* for altering FAP fate and promoting non-adipocyte differentiation, we added growth phase *MFAP5*-CM to the C3H10T1/2 and porcine SVF cells with adipogenic differentiation ability. Oil Red O staining revealed a significant reduction in lipid accumulation in C3H10T1/2 cells following *MFAP5*-CM treatment (Fig. 4-A). qRT-PCR and Western blot analysis demonstrated the downregulation of adipogenic-related genes and upregulation of fibroblast markers (Fig. 4-B, C and G). These findings were further validated in porcine SVF cells, where *MFAP5*-CM treatment also significantly inhibited lipid accumulation (Fig. 4-D), while reducing *ACTA2* expression (Fig. 4-E and G). To further validate these findings, we conducted RNA-seq analysis on *MFAP5*-CM-treated SVF cells, which revealed significant downregulation of adipogenic markers (*PPARG*, *CD36*, *AdipoQ*, and *PLIN1*) and upregulation of non-adipogenic markers (*TGFB1*, *POSTN*, *MYH11*, and *WNT5A*) (Fig. 4-H). Furthermore, KEGG pathway enrichment analysis of DEGs demonstrated significant enrichment of downregulated genes in the PPAR signaling pathway and fatty acid metabolism (Fig. 4-I). Concurrently, the expression of several mitochondrial biogenesis-related proteins, including PGC1A, UCP3, TOM20, and COX4 were upregulated in both C3H10T1/2 and SVF cells treated with *MFAP5*-CM (Fig. 4-J). Taken together, our results indicate that elevated *MFAP5* expression attenuates adipocyte development while promoting non-adipogenic fibroblast differentiation.

3.5. Overexpression of *MFAP5* inhibits the differentiation of preadipocytes into adipocytes and promotes nonadipocyte fibroblasts

To elucidate the role of *MFAP5*, we examined its expression pattern at various time points during SVF adipogenesis. Throughout adipogenesis, *AdipoQ* and *PPARG* expression was markedly upregulated (Appendix D-a), whereas *MFAP5* expression was substantially downregulated (Fig. 5-A). To investigate the impact of *MFAP5* overexpression on preadipocyte adipogenic capacity, we established stable *MFAP5*-expressing ISP4# cells, in which *MFAP5* overexpression significantly attenuated the expression of key adipogenic markers, *AdipoQ* and *PPARG* (Fig. 5-B). Oil Red O staining revealed that *MFAP5* overexpression impaired preadipocyte differentiation into mature adipocytes, which was further supported by the downregulation of adipogenic markers (Fig. 5-C and D). Furthermore, *MFAP5* overexpression upregulated the expression of FAP markers (*PDGFRA*, *SCA1*, and *DCN*) and fibroblast-associated genes (*ACTA2*, *CNN1*, *VIM*, *CTHRC1*, and *TGFB1*) (Fig. 5-D and E). Western blot analysis corroborated the mRNA findings, demonstrating that *MFAP5* overexpression suppressed PPARG while enhancing ACTA2 expression (Fig. 5-F; Appendix D-c). Notably, *MFAP5* overexpression also induced fibroblast-associated gene expression in undifferentiated ISP4# cells (Fig. 5-G and H; Appendix D-d). The upregulated genes of *MFAP5* positive cells were enriched in the thermogenesis and oxidative phosphorylation pathways in the cold exposure group. Consequently, we assessed the expression profiles of mitochondrial biogenesis and thermogenesis-related genes. *MFAP5* overexpression significantly upregulated the expression levels of mitochondrial biogenesis and thermogenesis-related genes (Fig. 5-I and J; Appendix D-e), along with a notable increase in mitochondrial activity (Fig. 5-K).

3.6. *MFAP5* promotes nonadipogenic lineages *via* the Hippo signaling pathway

To further elucidate the downstream mechanisms of *MFAP5* regulation, the MAPK signaling pathway was investigated, as it was significantly enriched among differentially downregulated genes in *MFAP5*-positive cells within dorsal subWATs during cold exposure (Appendix G-b). Western blot analysis confirmed our hypothesis by demonstrating that the phosphorylation of both ERK and p38 MAPK were significantly suppressed in overexpression-*MFAP5* (OE-MFAP5) ISP4# cells (Fig. 6-A). As shown in Fig. 6-B, the downstream effects of *MFAP5*-CM treatment appear to be independent of the MAPK signaling pathway.

KEGG pathway analysis of the upregulated genes in SVF cells treated with *MFAP5*-CM identified significant enrichment of the Hippo signaling pathway (Appendix E-b). YAP1, a key downstream effector of the Hippo signaling pathway, is translocated to the nucleus in its non-phosphorylated state to regulate target gene expression (Huang *et al.* 2005). Western blot analysis demonstrated significant upregulation of YAP1 in both SVF and C3H10T1/2 cells, accompanied by an inhibition of phosphorylated YAP1 (p-YAP1) in SVF cells, while p-YAP1 levels remained unchanged in C3H10T1/2 cells (Fig. 6-C). Furthermore, *MFAP5* overexpression markedly upregulated YAP1 expression in ISP4# cells while concurrently suppressing p-YAP1 levels (Fig. 6-D). The expression of connective tissue growth factor (*CTGF*), a

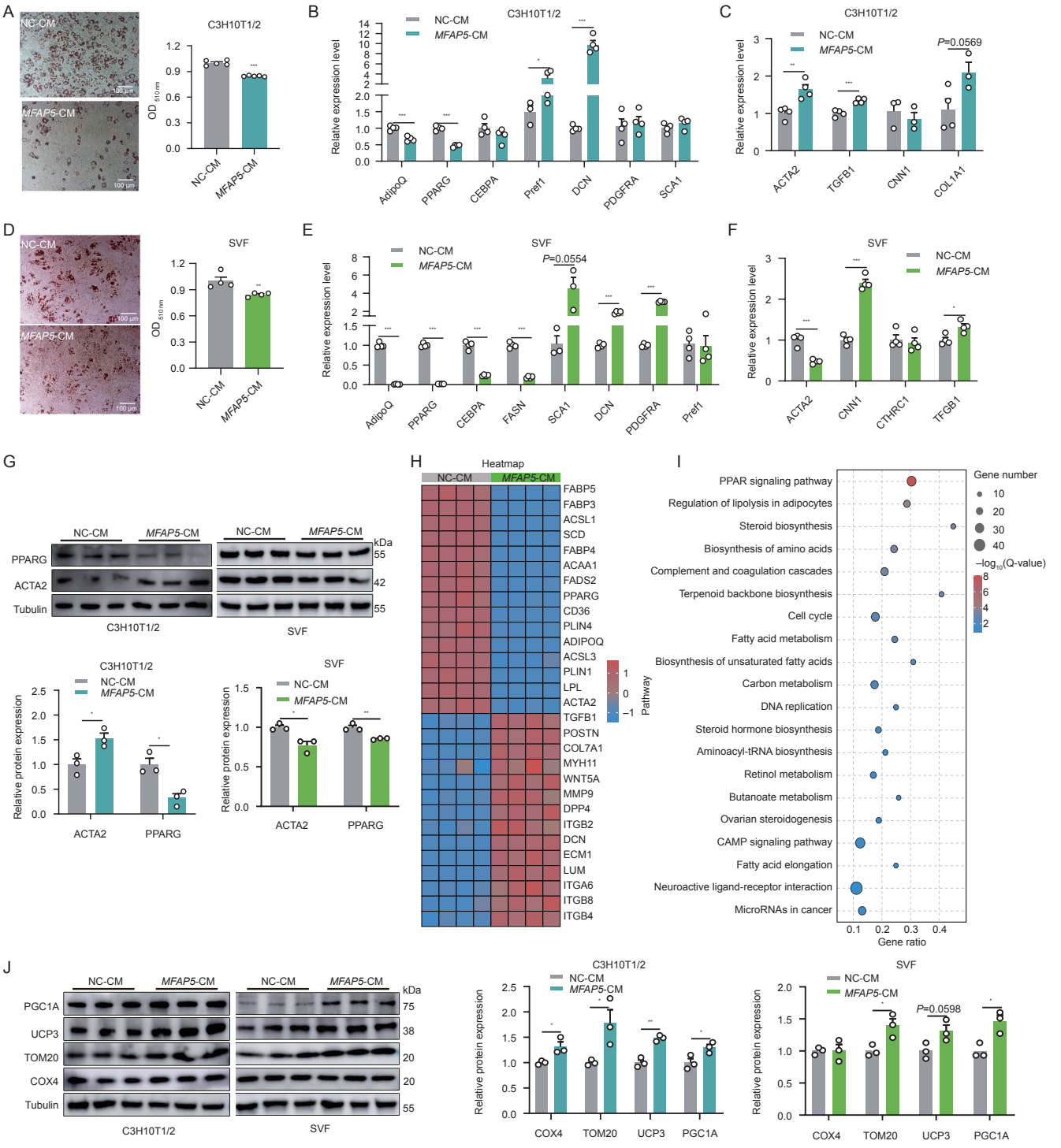

Fig. 4 The functional role of *MFAP5* conditioned medium in adipocytes. A–C, addition of control vector conditioned medium and overexpressing *MFAP5* conditioned medium for culturing immortalized porcine preadipocytes (ISP4#) to C3H10T1/2 cells, and subjected to differentiation. On d 8 of differentiation, cells were harvested and subjected to either an Oil Red O staining assay (n=5 biologically independent samples) (A) or qRT-PCR analysis (n=3–4 biologically independent samples) (B and C). Scale bar=100 μm. D–F, addition of control vector conditioned medium and *MFAP5*-overexpressing conditioned medium for culturing ISP4# to stromal vascular fraction (SVF) cells, and subjected to differentiation. On d 8 of differentiation, cells were harvested and subjected to either an Oil red O staining assay (n=4 biologically independent samples) (D) or qRT-PCR analysis (n=3–4 biologically independent samples) (E and F). Scale bar=100 μm. G and J, addition of control vector conditioned medium and *MFAP5*-overexpressing conditioned medium for culturing ISP4# to C3H10T1/2 and SVF cells, and subjected to differentiation. On d 8 of differentiation, cells were harvested and subjected to Western blot (n=3 biologically independent samples). H, heatmap constructed based on the RNA-seq data (samples with added control vector conditioned medium and *MFAP5*-overexpressing conditioned medium in SVF cells) for genes involved in adipogenesis and fibrogenesis. I, top 20 enrichment pathways revealed by KEGG enrichment analysis of the downregulated differentially expressed genes (DEGs) in SVF samples. All numerical values are presented as mean±SEM; two-tailed unpaired Student's *t*-test *P*-values are indicated as: *, $P \le 0.05$; **, $P \le 0.01$; ***, $P \le 0.001$.

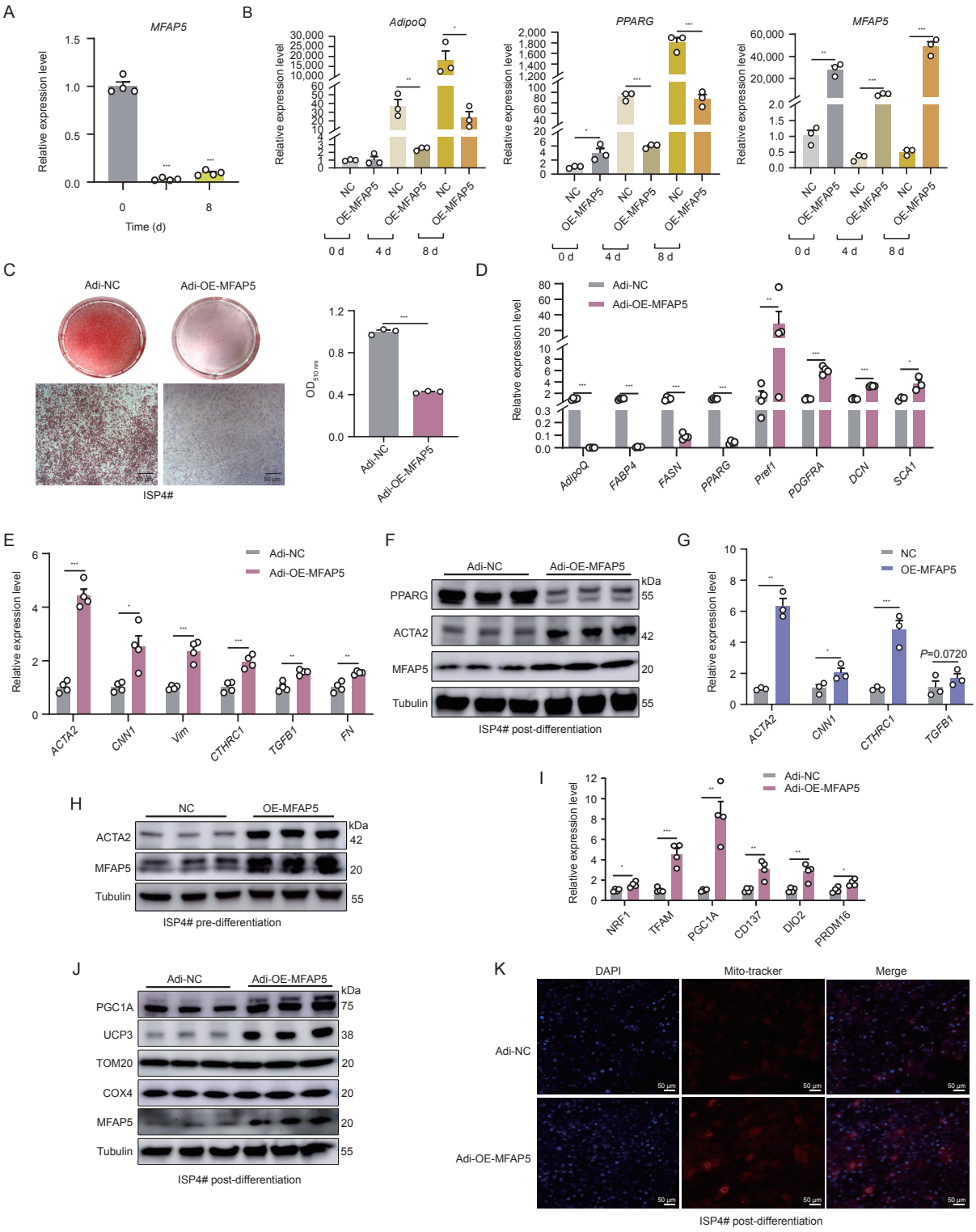

Fig. 5 The functional role of *MFAP5* in immortalized porcine preadipocytes (ISP4#) cells. A, porcine stromal vascular fraction (SVF) cells were subjected to adipocyte differentiation and harvested on d 0, 4, and 8 for qRT-PCR analysis of the *MFAP5* genes (n=4 biologically independent samples). B, control or *MFAP5*-overexpression ISP4# cells were set up and subjected to adipocyte differentiation and harvested on d 0, 4, and 8 for qRT-PCR analysis of the *AdipoQ*, *PPARG*, *MFAP5* genes (n=3 biologically independent samples). C–F, control or *MFAP5*-overexpression ISP4# cells were set up and subjected to differentiation. On d 8 of differentiation, cells were harvested and subjected to Oil Red O staining assay (n=3 biologically independent samples) (C), qRT-PCR analysis (n=3–4 biologically independent samples) (D and E), and Western blot (n=3 biologically independent samples) (F). Scale bar=50 μm. G and H, control or *MFAP5*-overexpression ISP4# preadipocyte were set up and harvested during cell contact inhibition for qRT-PCR analysis and Western blot (n=3 biologically independent samples). I–K, control or *MFAP5*-overexpression ISP4# cells were set up and subjected to differentiation. On d 8 of differentiation, cells were harvested and subjected to qRT-PCR analysis (n=4 biologically independent samples), Western blot (n=3 biologically independent samples) and mitochondrial activity detection. Scale bar=50 μm. All numerical values are presented as mean±SEM; two-tailed unpaired Student's t-test P-values are indicated as: *, $P\leq0.05$; **, $P\leq0.01$; ***, $P\leq0.001$.

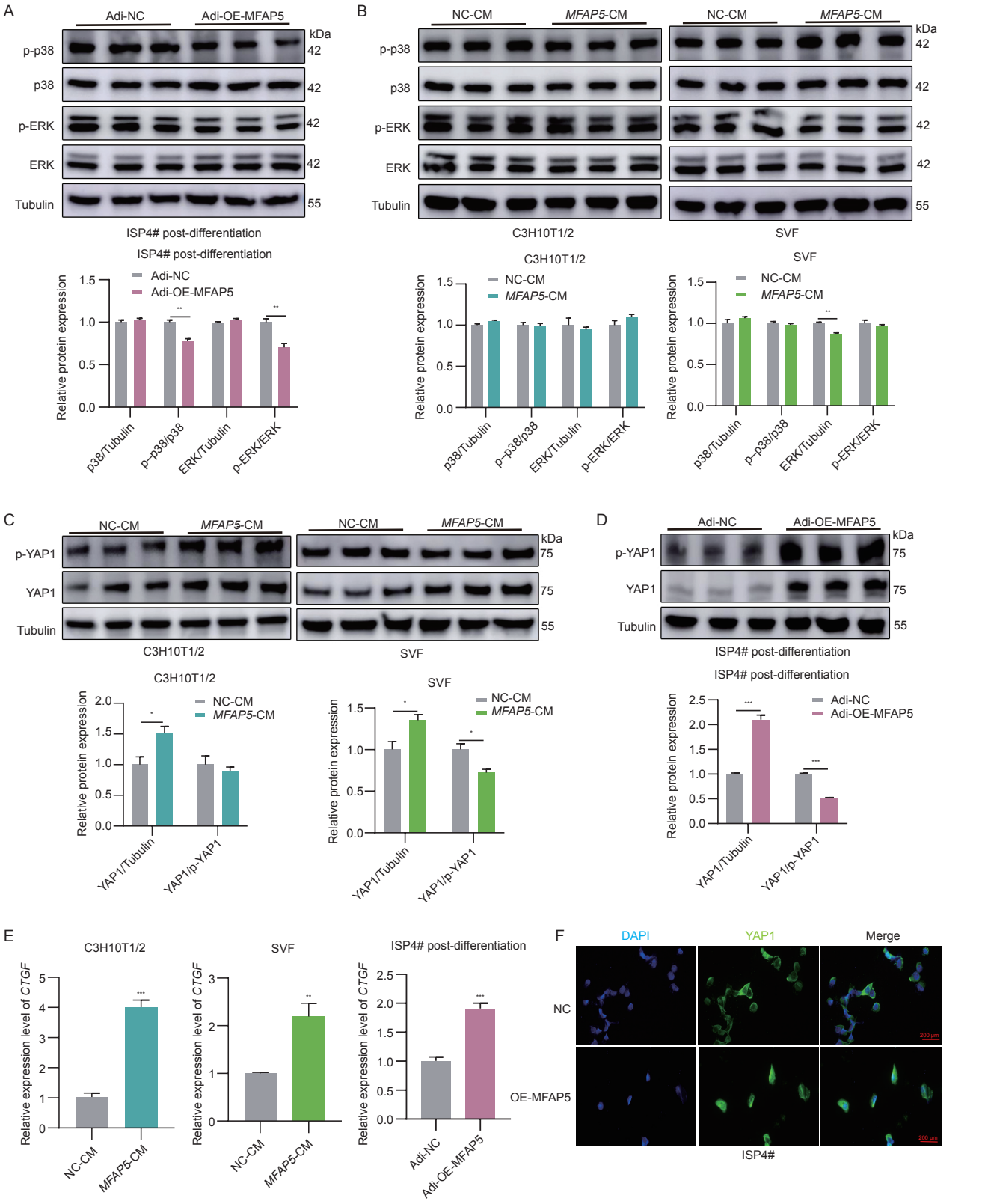

Fig. 6 *MFAP5* exerts its biological functions mainly through the Hippo signaling pathway. A and D, control or *MFAP5*-overexpression immortalized porcine preadipocytes (ISP4#) cells were set up and subjected to differentiation. On d 8 of differentiation, cells were harvested and subjected to Western blot (n=3 biologically independent samples). B and C, addition of control vector conditioned medium and *MFAP5*-overexpressing conditioned medium for culturing ISP4# to C3H10T1/2 and stromal vascular fraction (SVF) cells, and subjected to differentiation. On d 8 of differentiation, cells were harvested and subjected to Western blot (n=3 biologically independent samples). E, qRT-PCR analysis of *CTGF* gene expression in C3H10T1/2 and SVF adipocytes with the addition of control vector conditioned medium and *MFAP5*-overexpressing conditioned medium, and control or *MFAP5*-overexpression ISP4# cells (n=4 biologically independent samples). F, localization of YAP1 in ISP4# cells. Scale bar=200 μm. All numerical values are presented as mean±SEM; two-tailed unpaired Student's t-test P-values are indicated as: *, P≤0.05; **, P≤0.01; ***, P≤0.001.

downstream target gene of the Hippo signaling pathway, was significantly upregulated, suggesting the activation of the Hippo signaling pathway by *MFAP5* (Fig. 6-E) (Tamura *et al.* 2021; Wu *et al.* 2024). The *MFAP5* overexpression exhibited significantly enhanced nuclear fluorescence intensity of YAP1, suggesting that *MFAP5* promotes YAP1 nuclear translocation to mediate its biological effects (Fig. 6-F). Collectively, these findings demonstrate that *MFAP5* primarily mediates its biological effects through the Hippo signaling pathway.

4. Discussion

Cold exposure is a major challenge in piglet breeding, and the cold resistance of piglets is a widely sought trait among breeders. The Erhualian pig is a local pig breed in China, known for its high yield, high fat content, and excellent meat quality (Li *et al.* 2017; Xie *et al.* 2023). However, the response of Erhualian pigs with a large litter size to cold exposure has not been described yet. Therefore, we analyzed the responses of their adipose tissue to cold exposure, which will help us to understand the regulatory mechanism of cold resistance traits and has certain reference significance for the breeding of Erhualian pigs.

Previous studies have reported the presence of beige fat in the inguinal, perirenal, and axillary adipose tissues of Chinese cold resistant pig breeds during acute cold stimulation (Lin *et al.* 2017). As far as we know, this study provides the first comprehensive evaluation of the thermogenic potential of adipose tissue in various parts of pigs. In this study, the adipose tissues of ten parts of Erhualian pigs were studied during cold exposure and that the subcutaneous, inguinal, and deep neck adipose tissues of Erhualian pigs were found to have thermogenic potential. This is not entirely consistent with previous studies on adipose tissues in regions with thermogenic potential. This inconsistency may have arisen because our cold exposure cycles and temperatures were different and the breeds of pigs were different, but it also indicates that groin adipose is the most commonly reported adipose part that has resistance to cold.

Interestingly, we observed for the first time the appearance of brown adipose like cells and microfibers in the subWATs of the dorsal region of Erhualian pigs after cold exposure, but it is unclear whether these changes can contribute to cold resistance. An snRNA-seq and RNA-seq combined analysis identified *MFAP5* as a candidate gene. *MFAP5* is one of the DEGs shared by nonadipogenic fibroblasts subgroups (FAP1, FAP5, and FAP7 subgroups). Here we report that the overexpression of *MFAP5* or addition of *MFAP5*-CM inhibits the expression of adipogenic genes in adipogenic cells, while promoting gene expression in adipocyte stem cells and fibroblasts, indicating that MFAP5 can reverse the fate of adipocytes. *MFAP5* is expressed in the extracellular matrix (ECM) of human adipose tissue and is believed to be involved in the assembly of microfibrils and the composition of elastin (Lemaire *et al.* 2007; Vaittinen *et al.* 2015). Excessive ECM components can limit the swelling ability of adipocytes (Lin *et al.* 2016; Huan-Xian *et al.* 2023), and our results are consistent with early studies showing a negative correlation between *MFAP5* and adipogenic differentiation (Zhang *et al.* 2023). FAPs are stem cells that differentiate into adipocytes and fibroblasts (Maniyadath *et al.* 2023). In our results, the FAP1, FAP5, and FAP7 subgroups (nonadipogenic fibroblasts subgroups) were not derived from source proliferation, but rather from the differentiation of stem cells with adipogenic potential. Studies have reported that nonadipogenic lineages obtained through transdifferentiation are the main contributors to the extracellular matrix of adipocytes (Datta *et al.* 2018). *MFAP5* is often used as a fibroblast marker (Valenzi *et al.* 2019; Peng *et al.* 2023). Recombinant *MFAP5* can significantly enhance collagen contractility and pro-fibrosis gene expression in dermal fibroblasts (Han *et al.* 2023), and targeting MFAP5 with an immunologic approach can inhibit fibrosis in ovarian and pancreatic cancer (Yeung *et al.* 2019). Adding MFAP5-CM to porcine SVF cells resulted in the upregulation of other fibroblast genes such as *TGFB1*, *POSTN*, *MYH11*, but the inhibition of *ACTA2*. Studies have reported that adding ASC-conditioned medium to TGFβ-induced myofibroblasts inhibits *ACTA2* expression due to the secretion of BMP4 from ASCs (Hoerst *et al.* 2019). It is interesting that the addition of *MFAP5*-CM did not promote fibroblast gene expression in C2C12 cells without adipogenic ability, although it promoted C2C12 myogenic differentiation. However, its detailed mechanism deserves further research in the future. We speculate that it may be influenced by other factors secreted by the *MFAP5* cell line, as adipocytes are highly active secretory cells that can secrete multiple factors which participate in various physiological processes (Villarroya *et al.* 2017; Ghesmati *et al.* 2024).

In our results, the overexpression of *MFAP5* or addition of *MFAP5*-CM promoted the upregulation of PGC1A, TOM20, COX4, and UCP3 in ISP4#, C3H10T1/2, and SVF. Studies have reported that the adaptive thermogenesis of cold resistant pigs mainly relies on UCP3, although PGC1A, TOM20, and COX4 are star molecules involved in mitochondrial biogenesis (Du *et al.* 2017; Jang *et al.* 2021; Zhang *et al*. 2022). Mitochondria are important organelles that maintain homeostasis in response to varying cellular demands, such as brown and beige adipose that contain a large amount of biologically active mitochondria when facing cold conditions (Ikeda *et al.* 2018; Shao *et al*. 2019). But suitable tools for determining whether these fibroblasts in pig adipose tissue have a thermogenic function are currently lacking. In this study, no pathway for the development of brown adipose tissue was detected, and no typical brown or beige adipose tissue morphology was observed.

Some reports have identified YAP in the Hippo signaling pathway as a regulatory factor for mitochondrial biogenesis. In human umbilical vein endothelial cells, YAP knockdown leads to the downregulation of PGC1A, thereby impairing mitochondrial biogenesis (Mammoto *et al*. 2018). In another study, Hippo signaling effector YAP induced mitochondrial biogenesis through the translation of *TFAM* in mouse skeletal muscle (Hwang *et al*. 2022). In this study, the appearance of fibrous tissue in adipose tissue after cold exposure was due to the development of *MFAP5*-positive cells into a nonadipocyte fibroblast lineage. The observed brown adipocyte like morphology should have arose after fat consumption, as the lipolysis genes *ATGL* and *HSL* were

significantly upregulated. Therefore, we speculate that the adipose tissue of Erhualian piglets mainly resists cold through changes in cell lineage leading to mitochondrial biosynthesis.

5. Conclusion

This study showed that the subWATs of the dorsal region underwent remodeling after cold exposure, with a reduction in adipocytes and an increase in the proportion of FAPs, and developed toward the nonadipogenic fibroblast lineages. The transformation of the progenitor cell lineage can promote mitochondrial biogenesis, which is beneficial for resisting cold. *MFAP5* is crucial for the transformation of adipocytes to the nonadipogenic fibroblast lineage. In summary, our results indicate that *MFAP5* plays an important role in adipocyte development and fate determination, providing new insights into the cold resistance of pig adipose tissue and contributing to future improvements in piglet production efficiency.

Acknowledgements

This work was supported by grants from the Joint Funds of the National Natural Science Foundation of China (U20A2052), the National Natural Science Foundation of China (32372853, 32170847), the Jiangsu Agriculture Science and Technology Innovation Fund, China (CX(23)3137). The graphical abstract figure support was provided by Figdraw.

Declaration of competing interest

The authors declare that they have no conflict of interest.

Declaration generative AI and AI-assisted technologies in the writing process

The authors declare that they did not use AI in the preparation and writing of this manuscript.

Ethical Approval

All animal studies complied with the regulations by the Institutional Animal Care and Use Committee (IACUC) of Nanjing Agricultural University, China.

Data availability

The snRNA-seq and RNA-seq datasets are deposited in the Genome Sequence Archive (Genomics, Proteomics & Bioinformatics 2021) in National Genomics Data Center, China (Nucleic Acids Res 2022), China National Center for Bioinformation/Beijing Institute of Genomics, Chinese Academy of Sciences (GSA: CRA020162, GSA: CRA020109, GSA: CRA042821) that are publicly accessible at https://ngdc.cncb.ac.cn/gsa.

Appendices are associated with this study are available at https://doi.org/10.1016/j.jia.2025.09.006

References

Berg F, Gustafson U, Andersson L. 2006. The uncoupling protein 1 gene (UCP1) is disrupted in the pig lineage: a genetic explanation for poor thermoregulation in piglets. *PLoS Genetics,* **2**, e129.

Bornstein M R, Neinast M D, Zeng X, Chu Q, Axsom J, Thorsheim C, Li K, Blair M C, Rabinowitz J D, Arany Z. 2023. Comprehensive quantification of metabolic flux during acute cold stress in mice. *Cell Metabolism*, **35**, 2077-2092.e2076.

Burl R B, Ramseyer V D, Rondini E A, Pique-Regi R, Lee Y H, Granneman J G. 2018. Deconstructing adipogenesis induced by β3-adrenergic receptor activation with single-cell expression profiling. *Cell Metabolism*, **28**, 300-309.e304.

Cheng Y M, Hong P C, Song M M, Zhu H N, Qin J, Zhang Z D, Chen H, Ma X Z, Tian M Y, Zhu W Y, Huang Z. 2023. An immortal porcine preadipocyte cell strain for efficient production of cell-cultured fat. *Communications Biology*, **6**, 1202.

Côté J A, Ostinelli G, Gauthier M F, Lacasse A, Tchernof A. 2019. Focus on dedifferentiated adipocytes: Characteristics, mechanisms, and possible applications. *Cell and Tissue Research*, **378**, 385–398.

Cristancho A G, Lazar M A. 2011. Forming functional fat: A growing understanding of adipocyte differentiation. *Nature Reviews. Molecular Cell Biology*, **12**, 722–734.

Cui H X, LUO N, Guo L P, Liu L, Xing S Y, Zhao G P, Wen J. 2023. TIMP2 promotes intramuscular fat deposition by regulating the extracellular matrix in chicken. *Journal of Integrative Agriculture*, **22**, 853–863.

Datta R, Podolsky M J, Atabai K. 2018. Fat fibrosis: friend or foe? *JCI Insight*, **3**, 19.

Le Dividich J, Noblet J. 1981. Colostrum intake and thermoregulation in the neonatal pig in relation to environmental temperature. *Biology of the Neonate*, **40**, 167–174.

Du K, Ramachandran A, Mcgill M R, Mansouri A, Asselah T, Farhood A, Woolbright B L, Ding W X, Jaeschke H. 2017. Induction of mitochondrial biogenesis protects against acetaminophen hepatotoxicity. *y. Food and Chemical Toxicology*, **108**, 339–350.

Ghesmati Z, Rashid M, Fayezi S, Gieseler F, Alizadeh E, Darabi M. 2024. An update on the secretory functions of brown, white, and beige adipose tissue: Towards therapeutic applications. *Reviews in Endocrine & Metabolic Disorders*, **25**, 279–308.

Han C, Leonardo T R, Romana-Souza B, Shi J, Keiser S, Yuan H, Altakriti M, Ranzer M J, Ferri-Borgogno S, Mok S C, Koh T J, Hong S J, Chen L, Dipietro L A. 2023. Microfibril-associated protein 5 and the regulation of skin scar formation. *Scientific Reports*, **13**, 8728.

He T, Wang S, Li S, Shen H, Hou L, Liu Y, Wei Y, Xie F, Zhang Z, Zhao Z, Mo C, Guo H, Huang Q, Zhang R, Shen D, Li B. 2023. Suppression of preadipocyte determination by SOX4 limits white adipocyte hyperplasia in obesity. *iScience*, **26**, 106289.

Hoerst K, Van Den Broek L, Sachse C, Klein O, Von Fritschen U, Gibbs S, Hedtrich S. 2019. Regenerative potential of adipocytes in hypertrophic scars is mediated by myofibroblast reprogramming. *Journal of Molecular Medicine* (Berlin, Germany), **97**, 761–775.

Hou L, Shi J, Cao L, Xu G, Hu C, Wang C. 2017. Pig has no uncoupling protein 1. *Biochemical and Biophysical Research Communications*, **487**, 795–800.

Hou L, Xie M, Cao L, Shi J, Xu G, Hu C, Wang C. 2018. Browning of pig white preadipocytes by co-overexpressing pig PGC-1α and mice UCP1. *Cellular Physiology and Biochemistry*, **48**, 556–568.

Huang J, Wu S, Barrera J, Matthews K, Pan D. 2005. The Hippo signaling pathway coordinately regulates cell proliferation and apoptosis by inactivating Yorkie, the *Drosophila* homolog of YAP. *Cell*, **122**, 421–434.

Hwang J H, Kim K M, Oh H T, Yoo G D, Jeong M G, Lee H, Park J, Jeong K, Kim Y K, Ko Y G, Hwang E S, Hong J H. 2022. TAZ links exercise to mitochondrial biogenesis *via* mitochondrial transcription factor A. *Nature Communications*, **13**, 653.

Ikeda K, Maretich P, Kajimura S. 2018. The common and distinct features of brown and beige adipocytes. *Trends in Endocrinology and Metabolism*, **29**, 191–200.

Jang E H, Lee J H, Kim S A. 2021. Acute valproate exposure induces mitochondrial Biogenesis and autophagy with FOXO3a modulation in SH-SY5Y cells. *Cells*, **10**, 2522.

Kelley K W, Blecha F, Regnier J A. 1982. Cold exposure and absorption of colostral immunoglobulins by neonatal pigs. *Journal of Animal Science*, **55**, 363–368.

Kotarsky C J, Johnson N R, Mahoney S J, Mitchell S L, Schimek R L, Stastny S N, Hackney K J. 2021. Time-restricted eating and concurrent exercise training reduces fat mass and increases lean mass in overweight and obese adults. *Physiolgical Reports*, **9**, e14868.

Krois C R, Vuckovic M G, Huang P, Zaversnik C, Liu C S, Gibson C E,

Wheeler M R, Obrochta K M, Min J H, Herber C B, Thompson A C, Shah I D, Gordon S P, Hellerstein M K, Napoli J L. 2019. RDH1 suppresses adiposity by promoting brown adipose adaptation to fasting and re-feeding. *Cellular and Molecular Life Sciences*, **76**, 2425–2447.

Lemaire R, Bayle J, Mecham R P, Lafyatis R. 2007. Microfibril-associated MAGP-2 stimulates elastic fiber assembly. *The Journal of Biological Chemistry*, **282**, 800–808.

Li P H, Ma X, Zhang Y Q, Zhang Q, Huang R H. 2017. Progress in the physiological and genetic mechanisms underlying the high prolificacy of the Erhualian pig. *Hereditas*, **39**, 1016–1024. (in Chinese)

Lin D, Chun T H, Kang L. 2016. Adipose extracellular matrix remodelling in obesity and insulin resistance. *Biochemical Pharmacology*, **119**, 8–16.

Lin J, Cao C, Tao C, Ye R, Dong M, Zheng Q, Wang C, Jiang X, Qin G, Yan C, Li K, Speakman J R, Wang Y, Jin W, Zhao J. 2017. Cold adaptation in pigs depends on UCP3 in beige adipocytes. *Journal of Molecular Cell Biology*, **9**, 364–375.

Lin W, Tang Y, Zhao Y, Zhao J, Zhang L, Wei W, Chen J. 2020. MiR-144-3p targets foxo1 to reduce its regulation of adiponectin and promote adipogenesis. *Frontiers in Genetics*, **11**, 603144.

Mammoto A, Muyleart M, Kadlec A, Gutterman D, Mammoto T. 2018. YAP1-TEAD1 signaling controls angiogenesis and mitochondrial biogenesis through PGC1α. *Microvascular Research*, **119**, 73–83.

Maniyadath B, Zhang Q, Gupta R K, Mandrup S. 2023. Adipose tissue at single-cell resolution. *Cell Metabolism*, **35**, 386–413.

Miller C N, Yang J Y, England E, Yin A, Baile C A, Rayalam S. 2015. Isoproterenol increases uncoupling, glycolysis, and markers of beiging in mature 3T3-L1 adipocytes. *PLoS ONE*, **10**, e0138344.

Newman A A C, Serbulea V, Baylis R A, Shankman L S, Bradley X, Alencar G F, Owsiany K, Deaton R A, Karnewar S, Shamsuzzaman S, Salamon A, Reddy M S, Guo L, Finn A, Virmani R, Cherepanova O A, Owens G K. 2021. Multiple cell types contribute to the atherosclerotic lesion fibrous cap by PDGFRβ and bioenergetic mechanisms. *Nature Metabolism*, **3**, 166–181.

Norreen-Thorsen M, Struck E C, Öling S, Zwahlen M, Von Feilitzen K, Odeberg J, Lindskog C, Pontén F, Uhlén M, Dusart P J, Butler L M. 2022. A human adipose tissue cell-type transcriptome atlas. *Cell Reports*, **40**, 111046.

O'mara A E, Johnson J W, Linderman J D, Brychta R J, Mcgehee S, Fletcher L A, Fink Y A, Kapuria D, Cassimatis T M, Kelsey N, Cero C, Sater Z A, Piccinini F, Baskin A S, Leitner B P, Cai H, Millo C M, Dieckmann W, Walter M, Javitt N B, *et al.* 2020. Chronic mirabegron treatment increases human brown fat, HDL cholesterol, and insulin sensitivity. *The Jounal of Clinical Investigation*, **130**, 2209–2219.

Peng Z, Ren Z, Tong Z, Zhu Y, Zhu Y, Hu K. 2023. Interactions between MFAP5 + fibroblasts and tumor-infiltrating myeloid cells shape the malignant microenvironment of colorectal cancer. *Journal of Translational Medicine*, **21**, 405.

Rockey D C, Weymouth N, Shi Z. 2013. Smooth muscle α actin (Acta2) and myofibroblast function during hepatic wound healing. *PLoS ONE*, **8**, e77166.

Shao M, Wang Q A, Song A, Vishvanath L, Busbuso N C, Scherer P E, Gupta R K. 2019. Cellular origins of beige fat cells revisited. *Diabetes*, **68**, 1874–1885.

Shook B A, Wasko R R, Mano O, Rutenberg-Schoenberg M, Rudolph M C, Zirak B, Rivera-Gonzalez G C, López-Giráldez F, Zarini S, Rezza A, Clark D A, Rendl M, Rosenblum M D, Gerstein M B, Horsley V. 2020. Dermal adipocyte lipolysis and myofibroblast conversion are required for efficient skin repair. *Cell Stem Cell*, **26**, 880-895.e886.

Tamura T, Kodama T, Sato K, Murai K, Yoshioka T, Shigekawa M, Yamada R, Hikita H, Sakamori R, Akita H, Eguchi H, Johnson R L, Yokoi H, Mukoyama M, Tatsumi T, Takehara T. 2021. Dysregulation of PI3K and Hippo signaling pathways synergistically induces chronic pancreatitis *via* CTGF upregulation. *The Journal of Clinical Investigation*, **131**, 13.

Trayhurn P, Temple N J, Van Aerde J. 1989. Evidence from immunoblotting studies on uncoupling protein that brown adipose tissue is not present in the domestic pig. *Canadian Journal of Physiology and Pharmacology*, **67**, 1480–1485.

Vaittinen M, Kolehmainen M, Rydén M, Eskelinen M, Wabitsch M, Pihlajamäki J, Uusitupa M, Pulkkinen L. 2015. MFAP5 is related to obesity-associated adipose tissue and extracellular matrix remodeling and inflammation. *Obesity* (Silver Spring), **23**, 1371–1378.

Valenzi E, Bulik M, Tabib T, Morse C, Sembrat J, Trejo Bittar H, Rojas M, Lafyatis R. 2019. Single-cell analysis reveals fibroblast heterogeneity and myofibroblasts in systemic sclerosis-associated interstitial lung disease. *Annals of the Rheumatic Diseases*, **78**, 1379–1387.

Vijay J, Gauthier M F, Biswell R L, Louiselle D A, Johnston J J, Cheung W A, Belden B, Pramatarova A, Biertho L, Gibson M, Simon M M, Djambazian H, Staffa A, Bourque G, Laitinen A, Nystedt J, Vohl M C, Fraser J D, Pastinen T, Tchernof A, *et al.* 2020. Single-cell analysis of human adipose tissue identifies depot and disease specific cell types. *Nature Metabolism*, **2**, 97–109.

Villarroya F, Cereijo R, Villarroya J, Giralt M. 2017. Brown adipose tissue as a secretory organ. *Nature Reviews: Endocrinology*, **13**, 26–35.

Winther S, Isidor M S, Basse A L, Skjoldborg N, Cheung A, Quistorff B, Hansen J B. 2018. Restricting glycolysis impairs brown adipocyte glucose and oxygen consumption. *American Journal of Physiology. Endocrinology and Metabolism*, **314**, E214–E223.

Wu Y, Li C S, Meng R Y, Jin H, Chai O H, Kim S M. 2024. Regulation of Hippo-YAP/CTGF signaling by combining an HDAC inhibitor and 5-fluorouracil in gastric cancer cells. *Toxicology and Applied Pharmacology*, **482**, 116786.

Xiao F, Jiang H, Li Z, Jiang X, Chen S, Niu Y, Yin H, Shu Y, Peng B, Lu W, Li X, Li Z, Lan S, Xu X, Guo F. 2023. Reduced hepatic bradykinin degradation accounts for cold-induced BAT thermogenesis and WAT browning in male mice. *Nature Communications,* **14**, 2523.

Xie X, Huang C, Huang Y, Zou X, Zhou R, Ai H, Huang L, Ma J. 2023. Genetic architecture for skeletal muscle glycolytic potential in Chinese Erhualian pigs revealed by a genome-wide association study using 1.4M SNP array. *Frontiers in Genetics*, **14**, 1141411.

Yeung T L, Leung C S, Yip K P, Sheng J, Vien L, Bover L C, Birrer M J, Wong S T C, Mok S C. 2019. Anticancer immunotherapy by MFAP5 blockade inhibits fibrosis and enhances chemosensitivity in ovarian and pancreatic cancer. *Clinical Cancer Research*, **25**, 6417–6428.

Zeve D, Seo J, Suh J M, Stenesen D, Tang W, Berglund E D, Wan Y, Williams L J, Lim A, Martinez M J, Mckay R M, Millay D P, Olson E N, Graff J M. 2012. Wnt signaling activation in adipose progenitors promotes insulin-independent muscle glucose uptake. *Cell Metabolism*, **15**, 492–504.

Zhang C, Fu Q, Shao K, Liu L, Ma X, Zhang F, Zhang X, Meng L, Yan C, Zhao X. 2022. Indole-3-acetic acid improves the hepatic mitochondrial respiration defects by PGC1a up-regulation. *Cellular Signalling*, **99**, 110442.

Zhang T, Li H, Sun S, Zhou W, Zhang T, Yu Y, Wang Q, Wang M. 2023. Microfibrillar-associated protein 5 suppresses adipogenesis by inhibiting essential coactivator of PPARγ. *Scientific Reports*, **13**, 5589.

Zheng Q, Lin J, Huang J, Zhang H, Zhang R, Zhang X, Cao C, Hambly C, Qin G, Yao J, Song R, Jia Q, Wang X, Li Y, Zhang N, Piao Z, Ye R, Speakman J R, Wang H, Zhou Q, *et al.* 2017. Reconstitution of UCP1 using CRISPR/Cas9 in the white adipose tissue of pigs decreases fat deposition and improves thermogenic capacity. *Proceedings of the National Academy of Sciences of the United States of America*, **114**, e9474–e9482.

Executive Editor-in-Chief Kui Li
Managing Editor Yanyan Sun